Geological Quarterly, 2025, 69, 39
DOI: https://doi.org/10.7306/gq.1812

Landslide susceptibility mapping in the western Słonne Góry (SE Poland): a comparative study of landslide polygons and buffer zones using the Frequency Ratio Method

Edyta RYCIO[1, *]

[1] Polish Geological Institute – National Research Institute, Geohazard Center, Skrzatów 1, 31-560 Kraków, Poland; ORCID: 0000-0002-6738-7567

Rycio, E., 2025. Landslide susceptibility mapping in the western Słonne Góry (SE Poland): a comparative study of landslide polygons and buffer zones using the Frequency Ratio Method. Geological Quarterly, **69**, 39; https://doi.org/10.7306/gq.1812

A high variability of landslide density and distribution was observed in the western part of the Słonne Góry (Sanok region, Eastern Carpathians, SE Poland). A statistical method, the bivariate Frequency Ratio Model (FRM), was used to show the reasons for this variability and to compile a map of landslide susceptibility for the study area. The landslide susceptibility map was calculated using an inventory of previous landslides and using buffer zones mapped around the upper parts of landslides. The polygons of landslides represented disturbed features and slope properties. In contrast, buffer zones represented undisturbed slope features and properties. Both methods gave similar results. Two landslide susceptibility maps were obtained with the following Area Under the Curve (AUC) values: 0.7936 for landslides and 0.7971 for buffer zones. This indicates a sufficiently good fit of the computational models for predicting new landslides. Unfortunately, the use of buffer zones in the calculations, which represent undisturbed slope properties, did not improve the predictive values of the susceptibility maps. Significant differences were shown as regards slope angle. The importance of this parameter (slope angle) for the Polish part of the Carpathians was better enhanced by the use of buffer zones in the landslide susceptibility calculations.

Key words: conditioning parameters, landslides, buffer zones, landslide susceptibility map, Frequency Ratio Model, Eastern Carpathians.

INTRODUCTION

It is considered that the development of landslides is influenced by the interaction of both passive and active geological and environmental factors (e.g., Bober, 1979, 1984; Dikau et al., 1996; Wójcik and Zimnal, 1996; Wójcik, 1997; Zabuski et al., 1999; Ziętara, 2006). The literature shows a dynamic development of various methods for calculating landslide susceptibility, hazard, and risk, as well as a worldwide increase in interest in this area. Scientists use maps, representing different properties and parameters of the slope on which landslides develop, for calculations, with primary reliance on landslide distribution maps (Carrara et al., 1991; Van Westen, 1993; Guzzetti et al., 1999; Mrozek et al., 2004; Długosz, 2011; Eeckhaut et al., 2012; Pradhan and Buchroithner, 2012; Pardeshi et al., 2013; Małka, 2015, 2021; Wojciechowski, 2019; Chen et al., 2020; Ou et al., 2021; Kamieniarz, 2022). Landsliding is a geological phenomenon that, within its boundaries, causes changes to the original shape and properties of the slope. This study uses the concept of the buffer zone, understood as a part of slope above the landslide with parameters undisturbed by mass movement (Süzen and Doyuran, 2004). This area represents the real (original) conditions of landslide development, and here I have mapped and analysed the buffer zones around the upper parts of the landslides studied. The idea of marking buffer zones had been considered several times, especially in Turkey. This approach was initiated and popularized by Süzen and Doyuran (2004) under the name “seed cells” theory (seed cell sampling strategy) (Yesilnacar and Topal, 2005; Yilmaz, 2007; Dagdelenler et al., 2016; Sahana and Sajjad, 2017; Zhang et al., 2020). To date, this methodology has not been implemented in Poland.

The aim of the study was to compare two computational models/methods for determining landslide susceptibility in the western part of the Słonne Góry (Słonne Mountains) and surrounding area located in the Eastern Carpathians, SE Poland. Calculations were performed using parameters taken from landslide polygons and buffer zones delineated around landslides. The method using landslide polygons is the most commonly used approach for assessing landslide susceptibility, hazard and risk, although polygons intersect with layers that represent environmental factors showing already-disturbed slope properties. This study compares these two computational methods and produces two index-based landslide susceptibility maps for the western part of the Słonne Góry, to identify the more effective computational variant, and to evaluate the importance of the designated buffer zones used in the calculations.

* E-mail: edyta.rycio@pgi.gov.pl

Received: April 29, 2025; accepted: September 23, 2025; first published online: November 19, 2025

The research hypothesis is that the buffer zone method will provide more accurate susceptibility maps.

So far in Poland, mainly bivariate and multivariate statistical methods using landslides have been used to calculate landslide susceptibility, hazard and risk. The most popular of these included the Index Method (Kamiński, 2007; Wojciechowski, 2009; Długosz, 2011; Świątek et al., 2014; Małka, 2015, 2021) and the Weight of Evidence Method (Mrozek et al., 2004; Kamiński, 2012; Mrozek, 2013; Wojciechowski, 2019; Wódka 2022a, b). More recently, the Frequency Ratio method has been applied by Grabowski et al. (2022) for the calculation of landslide susceptibility on the slopes of the lower Wisła Valley. Among multivariate statistical methods, the logistic regression method (Małka, 2021) and the empirical likelihood ratio function (ELR/LR) have also been introduced (Mrozek, 2013; Mrozek et al., 2016). Pioneering work was done by Kamieniarz (2022) who applied the AI method in order to calculate susceptibility and landslide hazards for the city of Kraków.

The use of buffer zones for calculating landslide susceptibility, hazard, and risk is less popular. The following approach, known as the Seed Cell Theory (or Seed Cell Sampling Strategy), was introduced when Süzan and Doyuran (2004) determined a 100-metre buffer around the main scarp and lateral scarps of a landslide. Parameters within the buffer zone were then used to compute susceptibility maps and validate computational models. Similarly, Yesilnacar and Topal (2005) determined a 100-metre buffer around the main scarp and lateral scarps of landslides. Six different training data sets were created by using the total number of buffer pixels and randomly selected pixels from landslide-free areas. These datasets were subsequently used for training and validating landslide susceptibility models which were built by the use of logistic regression methods. A different approach was used by Yilmaz (2007) who determined buffer zones with a width of 50 m, but divided them into 3 subsets. The data sets were created by using the seed cells of a main scarp (crowns) and a lateral scarp (flanks): only main scarp, and only lateral scarp. Each subset was used to generate landslide susceptibility maps using bivariate statistical methods, with the best results achieved using buffers above the main scarp. The methodology of using buffer zones in landslide susceptibility mapping was significantly modified by Dagdelenler et al. (2016) who determined buffers of 25, 50, 75 and 100 m around the upper parts of the landslides (approximately two-thirds of the landslide length). Using multivariate statistical methods (logistic regression), they calculated separate susceptibility maps for each buffer width, showing that the best results were obtained with a buffer width of 50 m.

Moreover, there is an approach where buffer zones are used in the final stages of the work to validate the susceptibility maps. Che et al. (2012) used a buffer width of 25 m. Alternatively, Yilmaz (2007) and Zhang et al. (2020) used the seed cell area index (SCAI) to validate the susceptibility maps which were calculated by the use of the pixels within buffer zones 50 and 20 m wide, respectively.

LOCATION OF THE STUDY AREA

The study area is located in southeastern Poland, in the Eastern Carpathians. It covers a total area of 55.38 km^2.

The predominant, central and eastern, parts of the study area belong to Słonne Góry. The smaller, northern part of the study area belongs to Garby Grabownickie (Grabownickie Hills), while the southwestern edges of the area belong to Obniżenie Sanockie (Sanok Depression; Fig. 1).

The main ridge lines follow the direction of the geological structures in the flysch bedrock, which are oriented NW–SE. The study area includes the San River gorge through the western part of the Słonne Góry. To the west of the San River gorge, the slopes are generally straight with a gentle slope of ~3–15° and an elevation ranging from 330 to 525 m a.s.l. To the east of the San River gorge, however, there are two ridges with distinct geomorphological features influenced by the geological structure. The ridge extending north of the Chochlański Stream (Fig. 1) has the character of a long, broad ridge with rounded, domed peaks reaching heights of 530 to 617 m a.s.l. The ridge south of the Chochlański Stream (Fig. 1), on the other hand, is characterized by a complex ridge line, significantly reshaped by numerous incised valleys. The ridges are generally narrow with conical peaks and elevations ranging from ~440 to 520 m a.s.l.

GEOLOGY OF THE STUDY AREA

The geological structure of the study area is depicted on the geological map (Fig. 2) and the lithostratigraphic profile (Fig. 3), which have been compiled based on two sheets of the Detailed Geological Map of Poland (DGMP) at a scale of 1:50,000, Sanok (1041) (Malata and Zimnal, 2013, 2014) and Tyrawa Wołoska (1042) (Malata and Rączkowski, 1996; Malata et al., 2016). Three main structural elements can be distinguished in the study area (Świdziński, 1953; Książkiewicz, 1972): the Silesian Nappe thrust over the Skole Nappe, and locally between them, the Sub-Silesian Nappe. Thus, the area exposes flysch formations characteristic of the Skole, Silesian, and Sub-Silesian units (Fig. 2). The deposits of the Silesian and Sub-Silesian units have been collectively described as the Silesian-Subsilesian units on account of common subdivisions, strong profile similarity, and interlocking deposits of both units in the study area. These are successions of sandstones, conglomerates, mudstones and shales of varying bed thicknesses, ranging in age from the Lower Cretaceous to the Lower Miocene. The flysch is locally overlain by Quaternary deposits, comprising clays, silts, sands, and gravels.

The extent of the main and secondary/minor overthrust zones, fold axes, and stratigraphic layer outcrops in this Carpathian region have a NW–SE orientation (Fig. 2). Faults in the study area predominantly trend NNE–SSW, less commonly NE–SW and are characterized by normal-slip and strike-slip displacements. These faults displace fold axes, overthrusts and stratigraphic unit outcrops. The largest fault zone is located between Sanok Biała Góra and Międzybrodzie Iłowate (Fig. 2), where the tectonic style of the study area changes.

CHARACTERISTICS OF LANDSLIDES IN THE SŁONNE GÓRY AND SURROUNDING AREA

During the geological fieldwork in the study area, 321 landslides with a total area of 5.21 km^2 were documented. The smallest of these has an area of 0.025 ha and the largest one of 26.11 ha. Landslides are not equally distributed in the study area. A higher density of landslides is observed in its central part, west of the San River gorge through the Słonne Góry, between the peaks of Kopacz, Pilnik, Horodna, Horodyszcze, Pańskie and Wroczeń (Fig. 4). Landslides of a large size as well as complex and rich internal relief have developed in this area. Only a few landslides of similar size and structure developed east of the San Valley. They formed in the range of hills be-

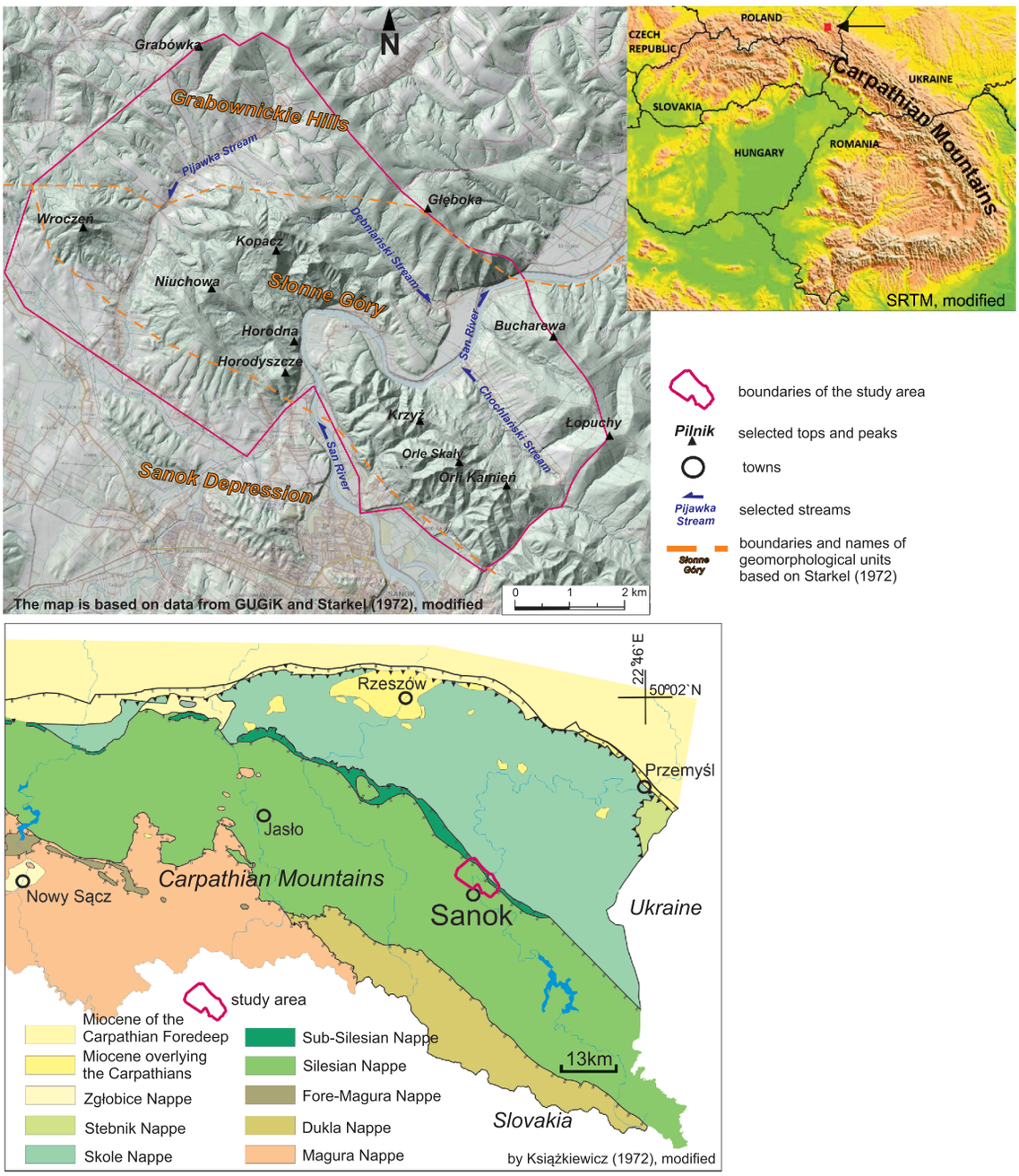

Fig. 1. Location of study area against background of the Carpathians, including the geomorphological regionalization according to Starkel (1972)

tween Mount Krzyż and Orli Kamień and on the southern slopes of Mount Bucharewa (Fig. 4). In the rest of the area, landslides are more scattered and smaller.

Most of the landslides in the Sanok area, especially large and deep ones, probably became active around the Pleistocene/Holocene boundary or in the Holocene during periods of increased humidity. Under these climatic conditions, a causal factor in the form of increased precipitation coincided with several favourable passive factors (Gil, 1997; Rączkowski and Mrozek, 2002; Gil and Długosz, 2006; Przyłucka and Karkowska, 2022). Increased precipitation is probably the main initiator of mass movements in the Słonne Góry.

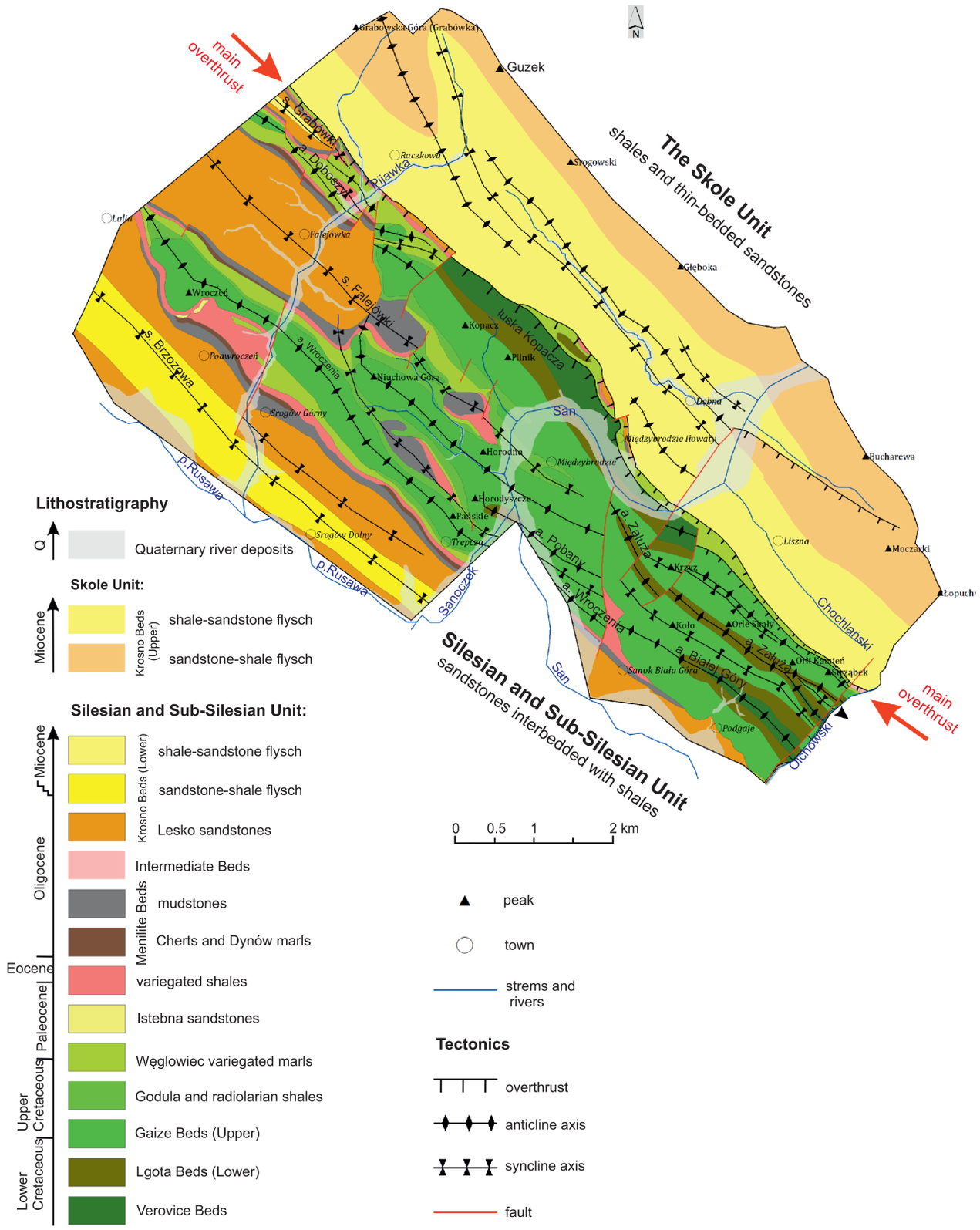

Fig. 2. Geological map of study area based on: Malata and Rączkowski (1996), Malata and Zimnal (2013, 2014), Malata et al., (2016), modified

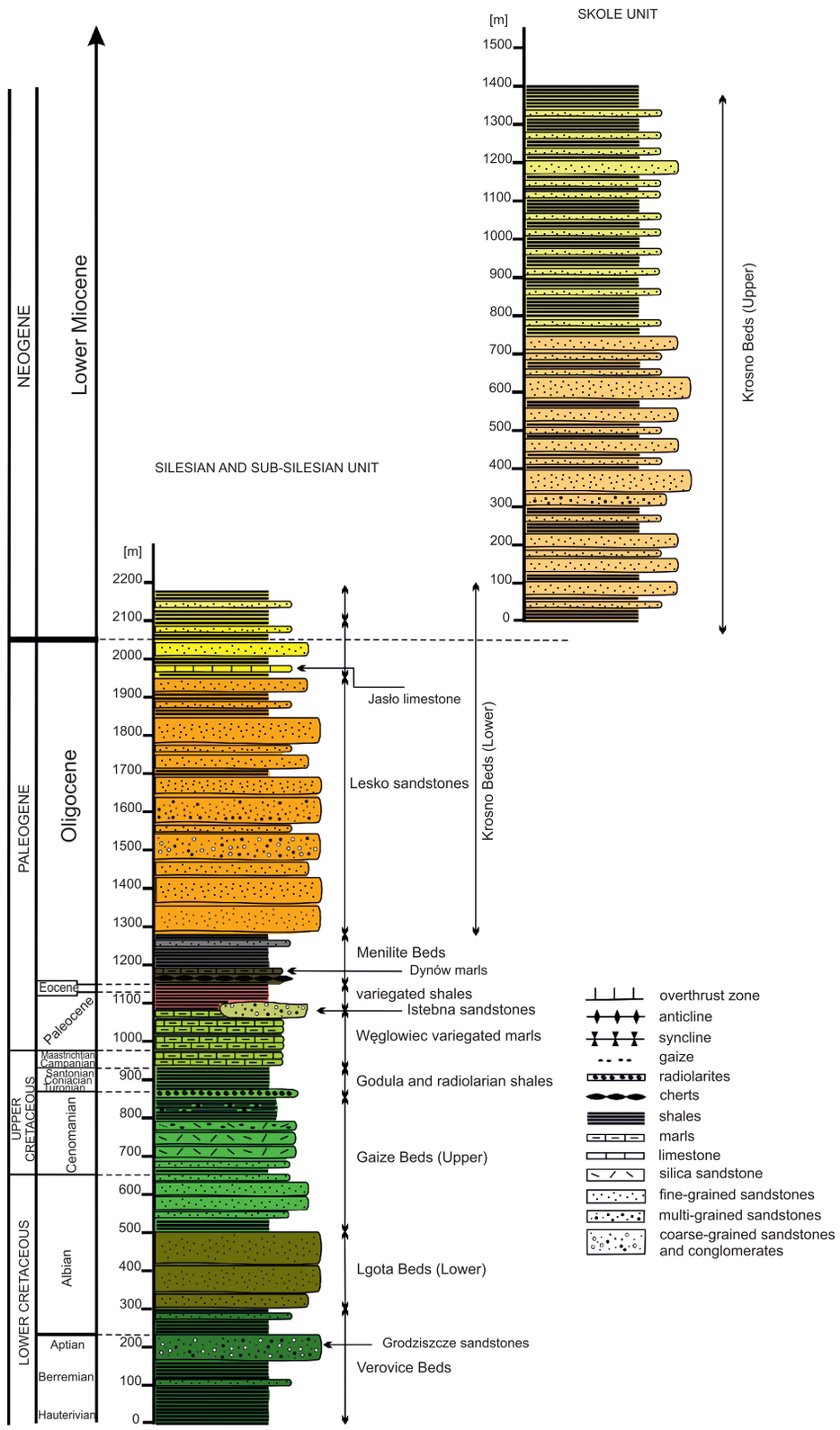

Fig. 3. Lithological and stratigraphic profile of geological strata in the study area

Profiles based on: Malata and Rączkowski (1996), Malata and Zimnal (2016, 2014), Malata et al. (2016), modified

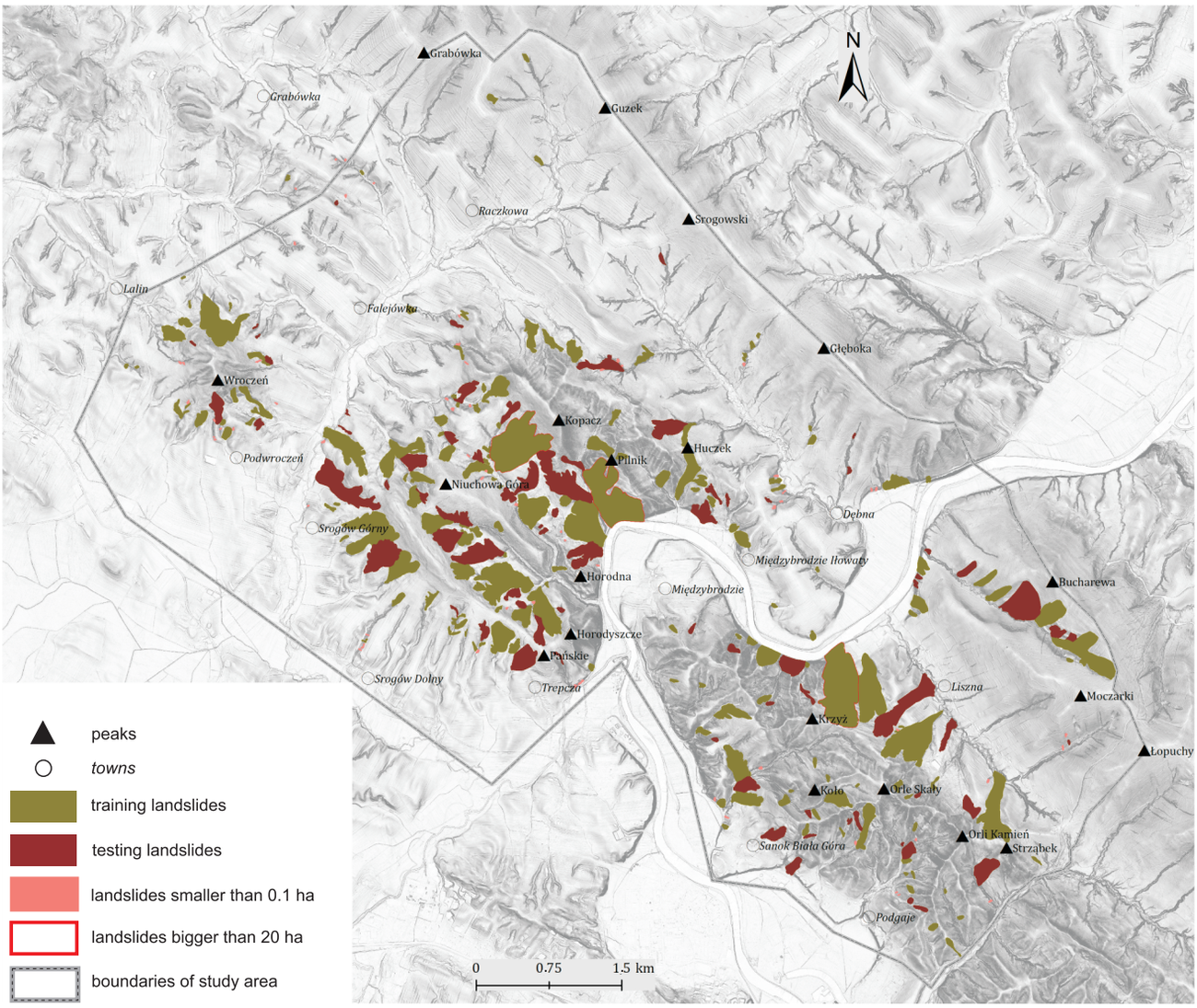

Fig. 4. Map of landslides in the study area

In order to characterize mass movements, the classification proposed by Margielewski (2009) has been used, which is based on the classification of Hutchinson (1968), Varnes (1978), WP/WLI (1990, 1993), Cruden and Varnes (1996), Dikau et al. (1996) and simultaneously refers to the Polish classifications of Kleczkowski (1955), Ziętara (1969), Bober (1984) and Zabuski et al. (1999). In the area analysed, slides dominate, accounting for a total of 50% of all mass movements. This is followed by complex landslides, which are a combination of different types of movement, accounting for 30%, and flows, accounting for 13% of all mass movements. In the landslide group, translational slides (26%) dominate over rotational slides (24%). Compound, non-rotational slides (Margielewski, 2009) account for 7% of the mass movements.

The most numerous group (63%) are landslides up to 1 ha in size, which altogether account for only 10% of the total landslide area. The largest total area is occupied by landslides in the 1–5 ha size class. These account for 27% of all landslides and altogether cover 32% of the landslide area in the study area. In the study area, 11 large landslides of >10 ha have been documented, which together constitute 41% of the total landslide area.

The surface landslide susceptibility and landslide density, defined and calculated according to the formula proposed by Bober (1984) for the entire study area, are 10.25% and 5.2 landslides/km^2, respectively.

RESEARCH METHODS

The decision to set a 40 m buffer was preceded by testing in zones with a width of 100 and 50 m, respectively. According to the suggestion of Dagdelenler et al. (2016), the 50 m wide buffer zone contained data which provided the best calculation results. Unfortunately, under the conditions of the study area selected, the initially determined wider buffer zones (100 and 50 m) contained too many areas unsuitable for calculation. They had to be excluded because, for instance, they were located outside a particular hydrographic divide or they included neigh-

bouring landslides. A buffer zone 40 m wide contains sufficient data on the original properties of the slope (before the landslide occurred) and the amount of data collected is statistically satisfactory. Wider buffer zones contained too much erroneous data, while narrower ones did not provide enough data for calculations. A 40 m buffer zone was found to be the optimal size through testing.

Buffers are located above the main scarp and on the sides of the two lateral scarps at their highest points. The following have been chosen because this is where the process of detachment of colluvial masses from the rock massif takes place. The buffer zones defined around the lower part of the landslide were excluded from the calculations because they contain lower parts of the slopes where colluvial material is accumulated rather than activated. The distribution of all buffer zones created and preserved is shown in Figure 5.

In pursuance of achieving the objective of this study, one of the bivariate statistical methods, the Frequency Ratio Model (FRM), has been used. This method involves observing the relationship between the distribution and density of landslides (or buffer zones) and each passive factor influencing the development of mass movements (Lee and Pradhan, 2007; Akgun, 2012; Mondal and Maiti, 2013; Huang et al., 2015; Ramesh, and Anbazhagan, 2015; Youssef, 2015; Nicu, 2018; Fayez et al., 2018; Khan et al., 2019; Silalahi et al., 2019). In this study, the following passive factors have been analysed: lithology, bedding-slope relationship, slope angle, slope aspect, distance from faults, distance from overthrusts and distance from fold axes. Each parameter was divided into several classes and represented graphically as a vector layer. Landslide Frequency Ratio (LFR) and Buffer Frequency Ratio (BFR) coefficients were then calculated for each class of passive factors identified according to the formulae:

$$\text{LFR} \quad \frac{\text{LF(landslide frequency)}}{\text{CF(class frequency)}} \quad \text{[formula 1]}$$

$$\text{LF} \quad \frac{\text{landslides in a given passive factor class in area (or pixels)}}{\text{total area (or the number of landslides in all classes of a given factor}} \quad \text{[formula 1a]}$$

$$\text{CF} \quad \frac{\text{area (or number of pixels) of a given class of passive factor}}{\text{total area (or the number of pixels) of all classes of passive factor}} \quad \text{[formula 1b]}$$

According to: Lee and Pradhan (2007), Huang et al. (2015), Ramesh and Anbazhagan (2015).

$$\text{BFR} \quad \frac{\text{BF(buffer frequency)}}{\text{CF(class frequency)}} \quad \text{[formula 2]}$$

$$\text{BF} \quad \frac{\text{area (or number of pixels) of the buffer zone in a given passive factor class}}{\text{total area (or the number of pixels) buffer zones in all classes of a given passive factor}} \quad \text{[formula 2a]}$$

A LFR/BFR value of 1 is the threshold value. The frequency ratio method assumes that an LFR or BFR value greater than 1 indicates a higher correlation, while a value less than 1 indicates a lower correlation of landslide occurrence with a given passive factor.

Furthermore, the Landslide Susceptibility Index (LSI) and the Buffer Susceptibility Index (BSI) have been calculated for each point in the study area using the formula:

$$\text{LSI} = \Sigma \text{LFRn} \quad \text{[formula 3a]}$$

$$\text{BSI} = \Sigma \text{ BFRn} \quad \text{[formula 3b]}$$

where: LFRn and BFRn are the FR coefficients of all (n) passive factors at a given location, taking into account landslides and buffer zones.

The values of the landslide and buffer susceptibility coefficients (LSI, BSI) represent the relative landslide susceptibility of the area. In this case, the higher the LSI and BSI values for a given area, the greater the landslide susceptibility and the greater the likelihood of future landslides. This method resulted in two index maps showing landslide susceptibility using LSI and BSI values.

In the final stage of the work, the two landslide susceptibility index maps obtained (LSI and BSI) were validated using a group of testing landslides to calculate the AUC prediction curve coefficient.

Vector values and polygon surface areas were used for the calculations. The total area of each passive factor layer is 50.33 km^2. This is the total area of the study area minus the areas of the flat river valleys.

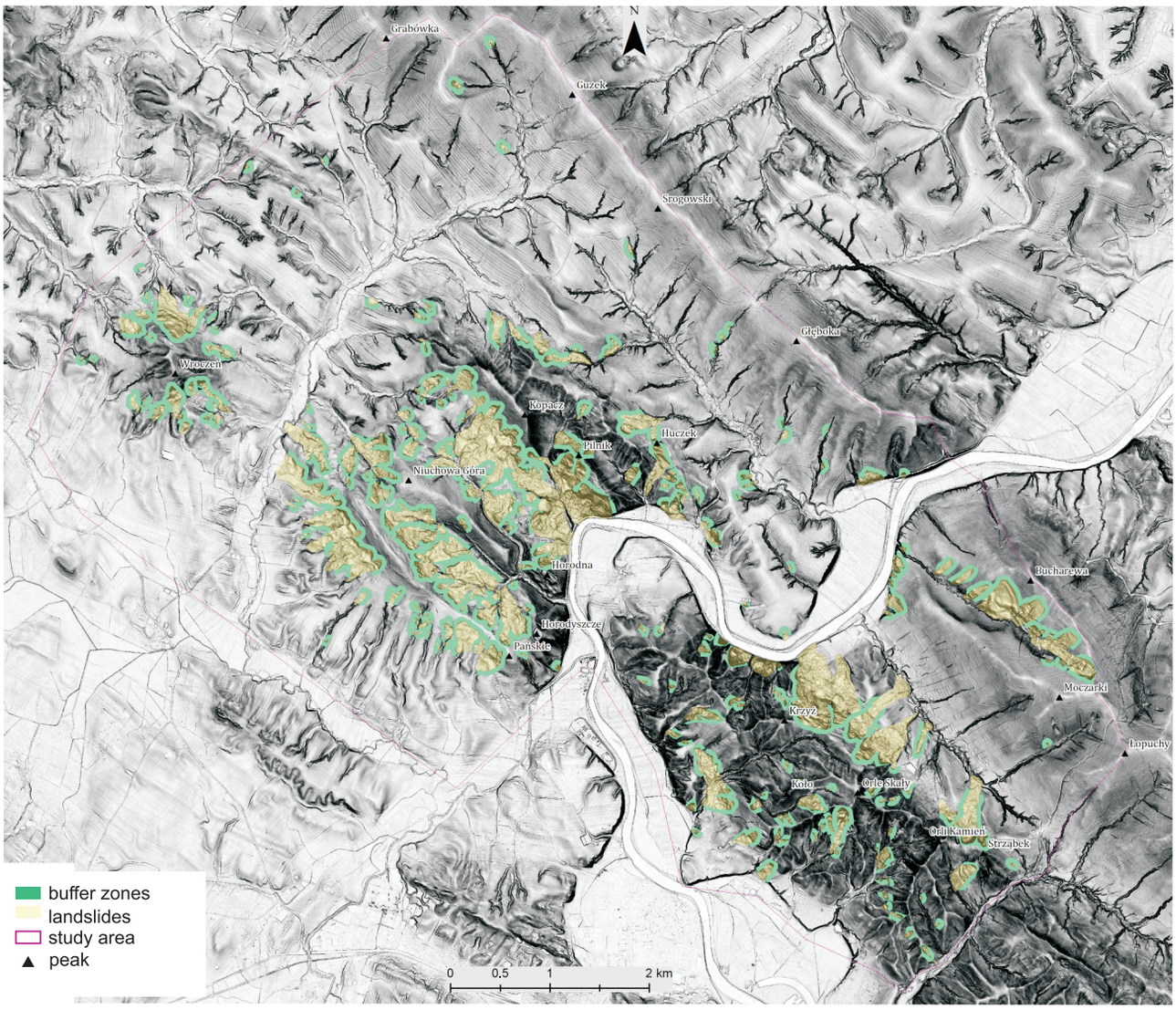

Fig. 5. Distribution of buffer zones in the study area

LAYERS USED FOR THE ANALYSIS

Landslide layer: landslides documented in the field have been divided into two groups. The first group of landslides used for susceptibility modelling contains 70% of all landslides, whereas the second group used for validation and testing of the model obtained contains 30% of landslides (Mrozek et al., 2004; Wojciechowski, 2009; Huang et al., 2015; Nicu, 2018; Zhang et al., 2020; Małka, 2021). The training landslides (sometimes referred to as calculated landslides) have been compiled on a separate polygon layer containing 183 landslides with a total area of 360.54 ha. The testing (validation) landslide layer contains 78 landslides with a total area of 156.28 ha (Fig. 4).

Buffer zones layer: used for the first time in Poland for this type of calculation. It consists of polygons with a total area of 304 ha. It shows the spatial distribution of 40 m buffer zones designated around the upper part of the landslides. The buffer layer was not divided into two sets (training and testing), but was used in its entirety to calculate the buffer frequency coefficients BFR (Fig. 5).

Geological layer (lithology): this shows the lithostratigraphic subdivisions of the area. It was developed on the basis of two DGMP 1:50,000 sheets, Sanok (1041) (Malata and Zimnal, 2014), and Tyrawa Wołoska (1042) (Malata et al., 2016). The geological structure, both lithological and tectonic, plays a significant role in the process of mass movement development, which was repeatedly corroborated by research (e.g., Bober, 1979, 1984, 1985, 1990a, b; Ziętara, 1991; Dikau et al., 1996; Wójcik and Zimnal, 1996; Zabuski et al., 1999; Margielewski, 2001; Długosz, 2011; Sikora, 2018; Wódka, 2019; Warmuz and Nescieruk, 2019; Kos, 2019; Kamieniarz, 2022; Fig. 6).

Bedding-slope relationship layer: this shows the spatial relationship between the slope surface (dip direction of slope) and the position of the rock bedding (dip direction of rock bedding) (Fig. 6). The slopes are divided into cataclinal (dip slope), anaclinal (anti-dip slope), transverse (transverse slope) and plagioclinal (cross-dip slope) (Grabowski et al., 2008; Chen et

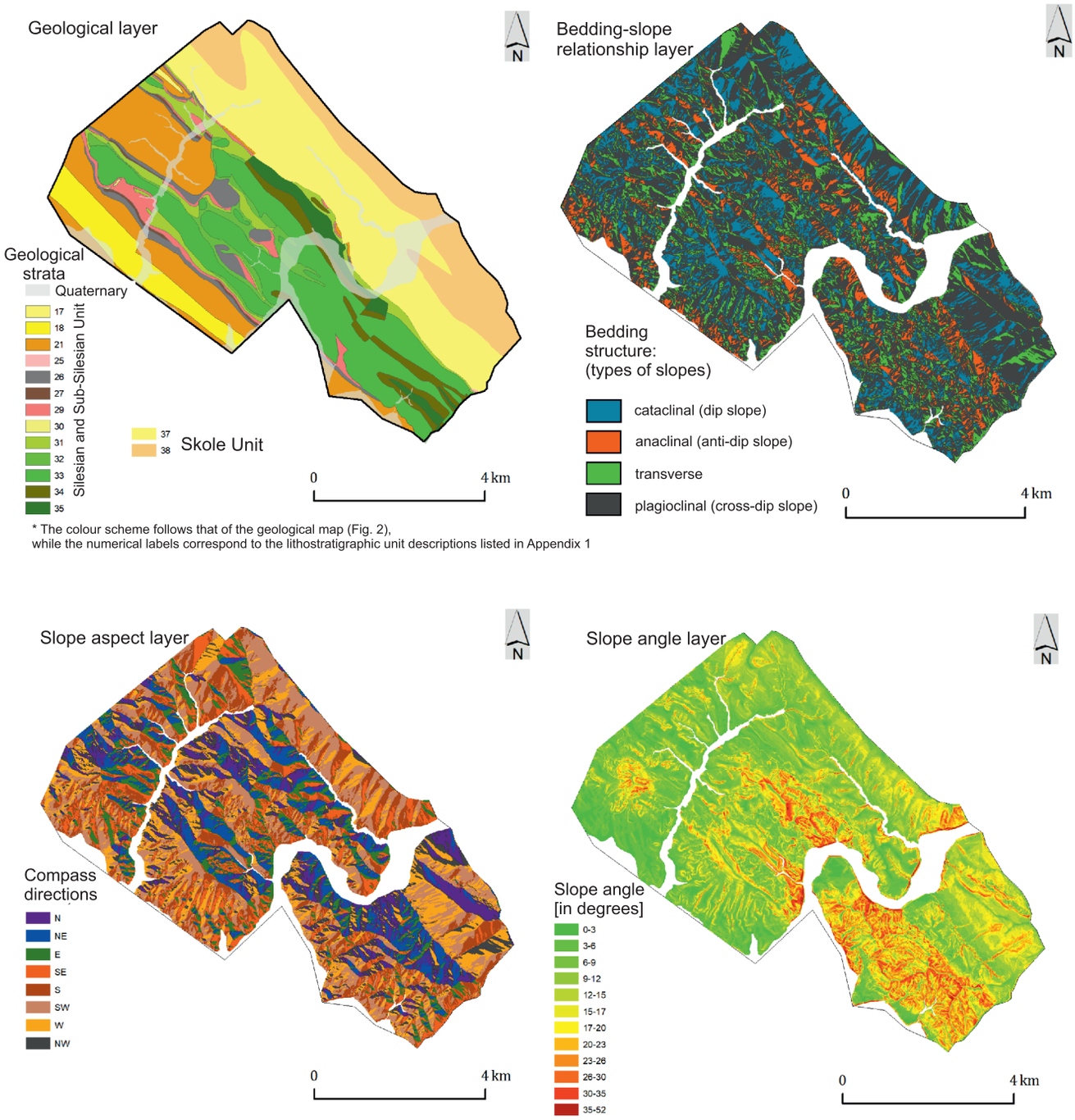

* The colour scheme follows that of the geological map (Fig. 2), while the numerical labels correspond to the lithostratigraphic unit descriptions listed in Appendix 1

Fig. 6. Maps showing the tectonic passive factors used in the GIS analysis

al., 2009). The group of plagioclinal slopes also includes parts of slopes with a complex and complicated arrangement of bedding planes associated with fault zones and thrust zones. This is the first attempt to show information on the bedding-slope relationship in a graphical and spatial way, so the coincidence of the slope azimuth and the azimuth of the rock bedding has been used, without taking the bedding dip angle and slope angle into account.

Slope aspect layer: this is expressed in degrees from 0–360° and represents the position of the slope surface in relation to the points of the compass and the sun (Fig. 6). The amount of sunlight and the strength of the wind, which depend on the slope aspect, indirectly affect precipitation, soil moisture and the duration of snow cover. It also affects the thickness and properties of weathering and soil.

Slope angle layer: this shows the angle of the slope surface. Slopes have a major influence on the development of mass movements. As the slope steepens, the shear forces in the rock mass increase (Fig. 6).

Tectonic layer: this shows elements of fold tectonics and disjunctive tectonics and the Euclidean distance to these structures (Fig. 7). Tectonics, in addition to and/or in combination

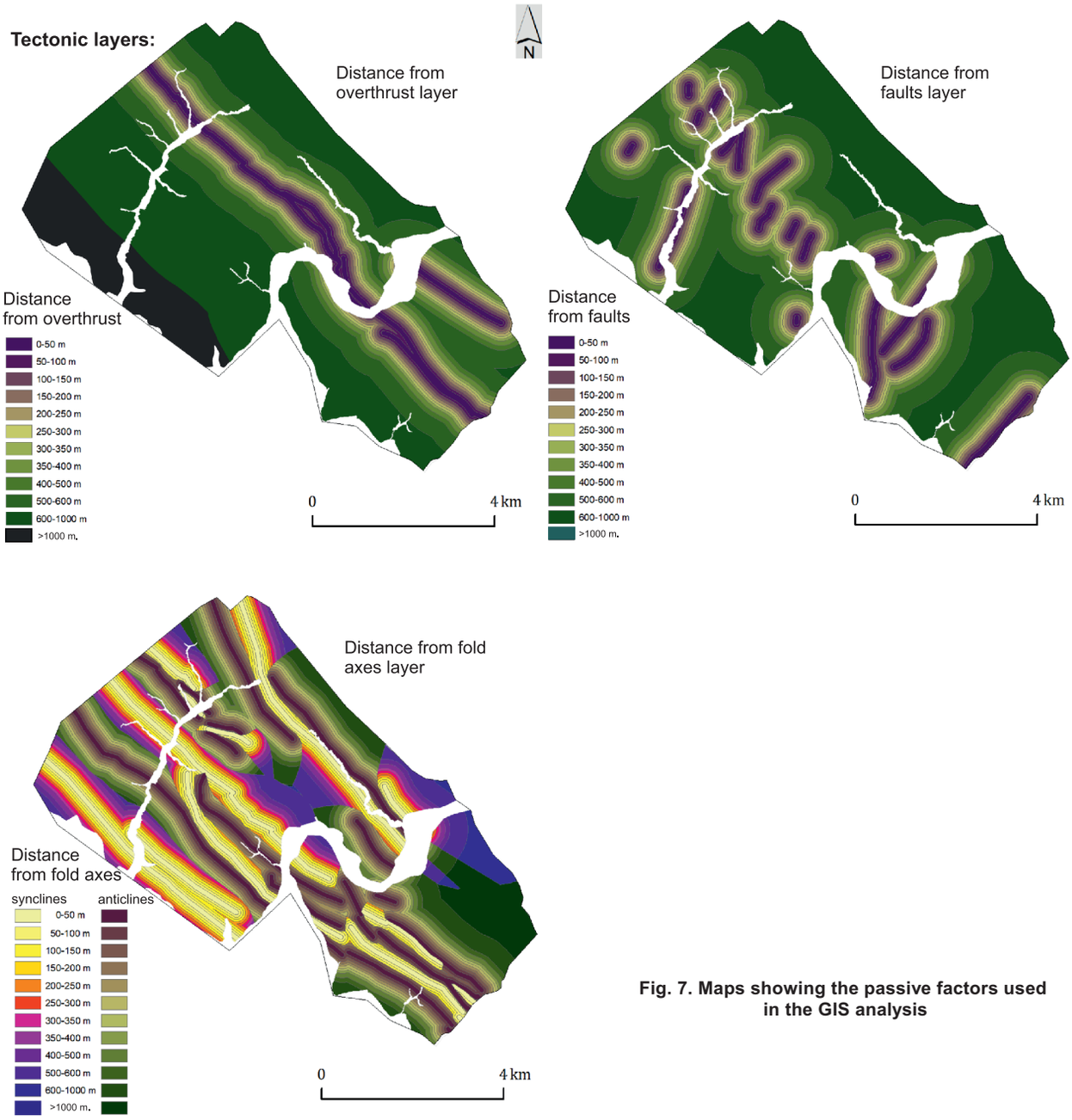

Fig. 7. Maps showing the passive factors used in the GIS analysis

with lithology, influences the development of landslides (Kleczkowski, 1955; Mastella, 1975; Bober, 1984; Wójcik and Zimnal, 1996; Zabuski et al., 1999; Długosz, 2011; Rycio, 2018; Sikora, 2018). Overthrust zones, fault zones, joint systems, bedding planes and (to a lesser extent) fold structures cause the rock mass to disintegrate and weaken its strength parameters. The fractured rock mass is more susceptible to weathering and absorbs water easily, affecting its weight and physico-mechanical properties. The tectonic map is shown in the form of 3 layers:

- layer of distances from overthrusts;
- layer of distances from faults;
- layer of distances from fold axes (synclines and anticlines), developed using the Euclidean assignment, which means that for each point on the terrain (for each pixel on the map) it has been calculated whether it is closer to the syncline axis or the anticline axis.

RESULTS

All passive factor layers (lithology, bedding-slope relationship, slope angle, slope aspect, distance from faults, overthrusts and fold axes) were crossed with the layer showing training landslides and with the layer of buffer zones. The intersection with the landslide layer resulted in the calculation of LFR coefficients according to formula 1, while the intersection with

the buffer zone layer resulted in BFR coefficients (according to formula 2) for all classes of passive factors determined.

As the results of the calculations in Appendix 1 show, the LFR and BFR coefficients differ within the classes. This is to be expected. Analysis of the LFR coefficients, derived from the training dataset, reveals that lithology, distance from faults, slope angle, distance from overthrusts, distance from fold axes, slope aspect, and the bedding-slope relationship are the dominant factors influencing landslide development (Fig. 8). The highest susceptibility occurs specifically on outcrops of Godulian and radiolarian shale, located within 50 m of fault or overthrust zones, where slope inclinations range from 35° to 52°. Furthermore, areas located 200–300 m from the anticline axis, particularly on north-facing slopes exhibiting a cataclinal (dip slope) structure, show a strong predisposition to mass movements.

However, according to the BFR coefficients obtained by the use of buffer zones, the order is slightly different and is as fol-

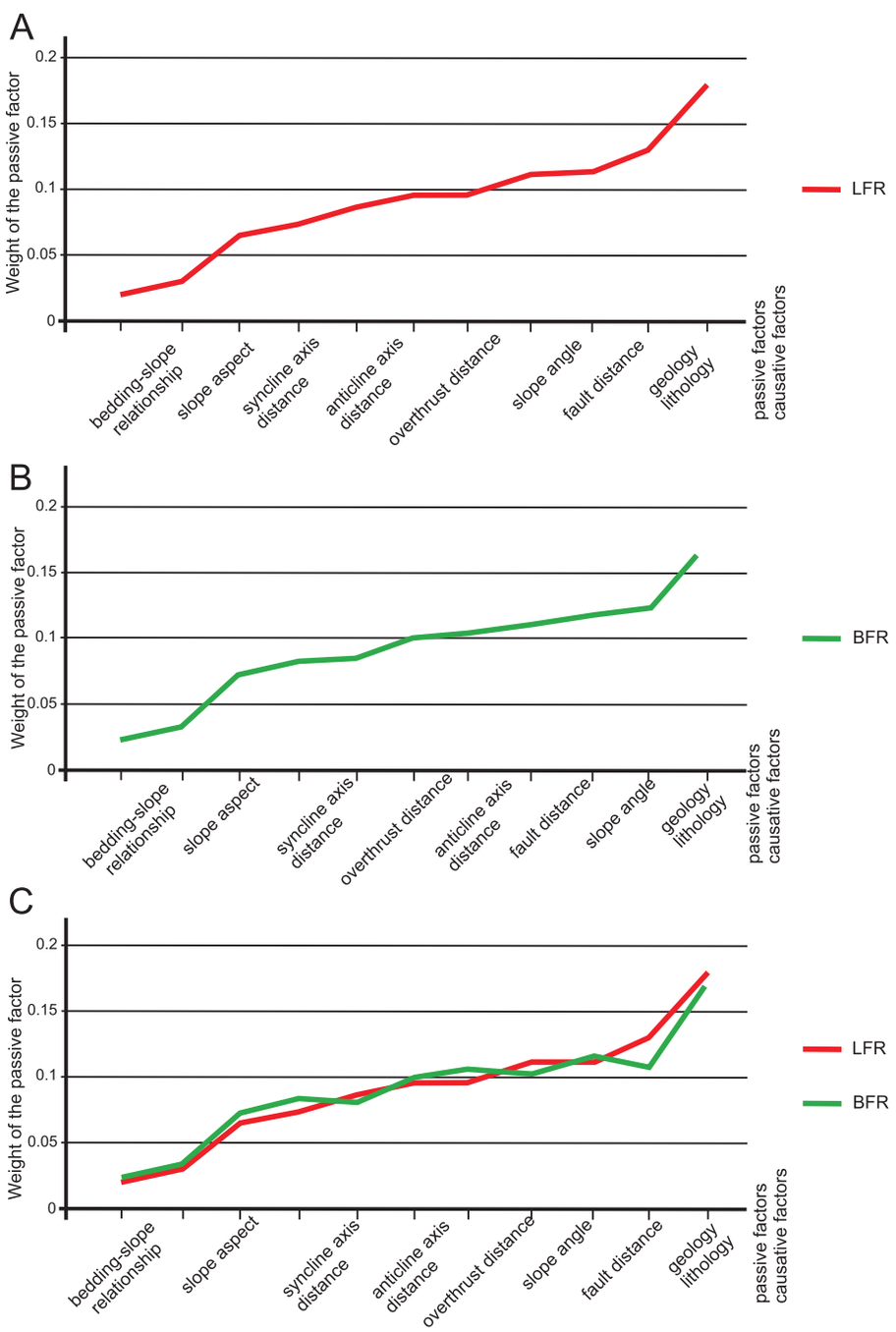

Fig. 8. Weight of passive factors and their comparison depending on the calculation method

lows: lithology, slope angle, distance from faults, distance from anticlines, distance from overthrusts, slope aspect, and bedding-slope relationship (Fig. 8). This calculation method also indicates the dominant influence of Godulian and radiolarian shales on the development of landslides. Favourable conditions exist on slopes with an angle of 17–23°, at a distance of 150–200 m from faults and anticline axes, and at a distance of 0–50 m from overthrusts. Slopes with NE exposure and cataclinal (dip slope) geological structure also favour the development of mass movements. The results are shown graphically in Figure 8. By comparing the results, it has been emphasised that in the western part of the Słonne Góry in Poland, the lithology of the flysch, the slope angle and the distance from faults have the greatest influence on the development of landslides. The bedding-slope relationship, the slope aspect and the distance from overthrust and fold axes are less relevant. Both methods provide similar results.

The ranking of the forty classes of passive factors with the highest LFR and BFR coefficients can be found in Appendix 2. When comparing the ranking of the highlighted classes, as much as 80% consistency was observed within the classes with the highest LFR and BFR coefficients. This result indicates the usefulness of using buffer zones in calculations, as it leads to similar results as in the case of calculations carried out using landslides.

LSI AND BSI INDEX MAPS

In the next step, the LFR and BFR coefficients obtained have been assigned to the corresponding classes of passive factors on vector layers, which are their graphical representations. Then, all passive factor layers have been summed to obtain LSI and BSI coefficients according to formulae 3a and 3b. The results are shown on the maps in Figure 9. Each pixel on the map is assigned an LSI or BSI coefficient value. The higher the value, the higher the susceptibility to landslides at a given location. Conversely, a lower LSI or BSI coefficient value indicates lower landslide susceptibility.

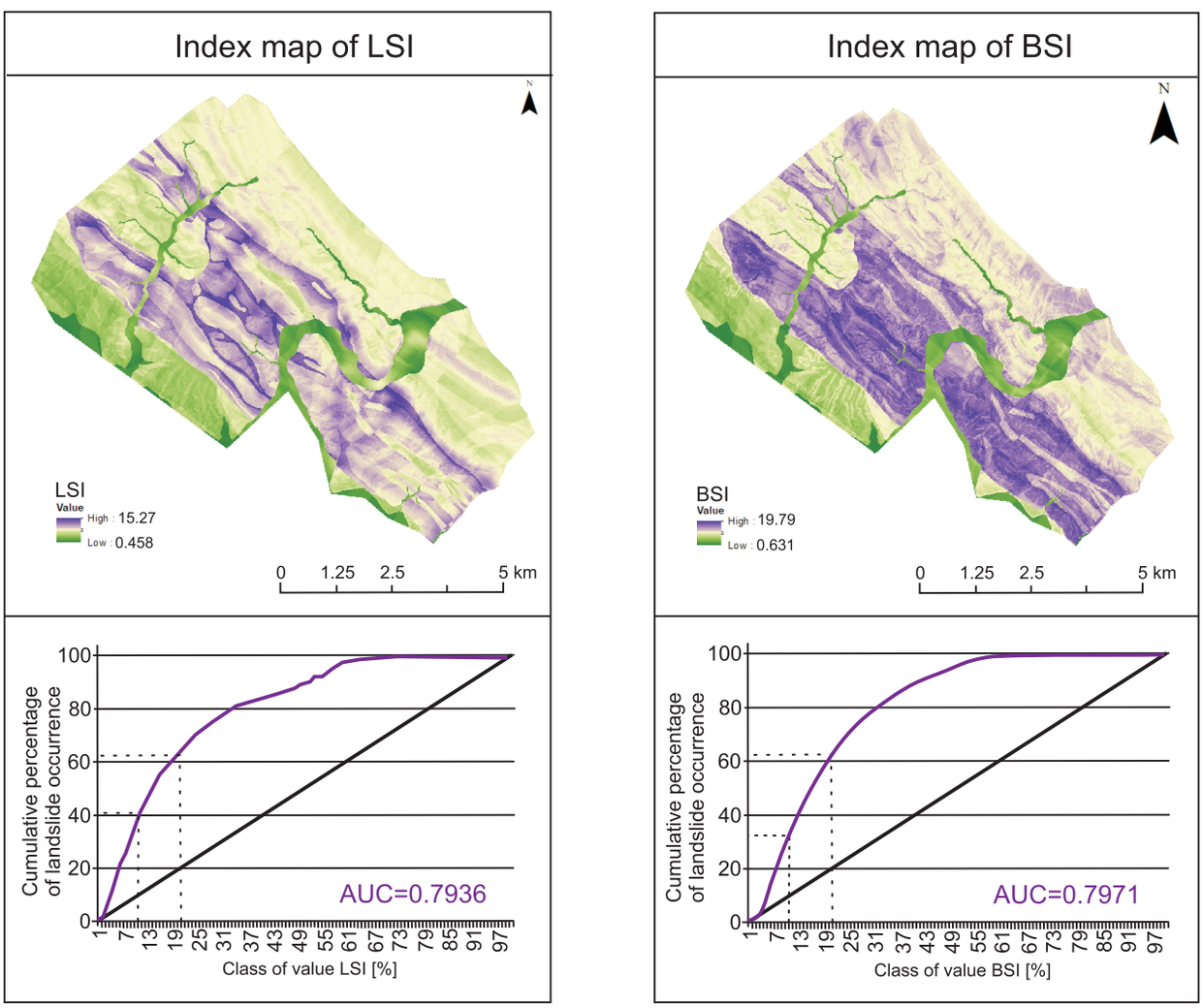

Fig. 9. Index maps of LSI and BSI with the Area Under the Curve (AUC) of their prediction curves

The resulting LSI and BSI index maps were verified, assuming geological timeliness, using a series of testing landslides not included in the previous coefficient calculations. The maps were intersected with the layer of test landslides to assess their predictive accuracy. This verification is essential to evaluate the reliability of the generated landslide susceptibility maps and their potential to predict future mass movements. The results indicate that new landslides tend to develop in areas most susceptible to mass movements — those with the highest LSI and BSI values. The verification resulted in a prediction curve and an Area Under the Curve (AUC) coefficient. The value of the AUC coefficient indicates the potential value of the landslide susceptibility index map obtained. The AUC coefficient is between 1 and 0, where AUC = 1 indicates a perfect fit or prediction of the model, and a value <0.6 indicates the unsuitability of the model. AUC coefficient values are often divided into 5 categories: 0.5–0.6 – means a wrong model, 0.6–0.7 – is a poor fit, 0.7–0.8 – is a sufficient fit, 0.8-0.9 is a good fit and 0.9–1.0 – is a perfect fit (Rabby and Li, 2020). The prediction curves and AUC values are shown in Figure 9.

An analysis of the obtained AUC coefficients at 0.7936 and 0.7971 showed that both calculation methods give similar results and have a similar predictive value, close to a sufficiently good and effective prediction of new mass movements. Only a more detailed analysis of the prediction curve shows slight differences in the effectiveness of the calculation methods used.

EVALUATION OF THE USEFULNESS OF BUFFER ZONES IN PREDICTING LANDSLIDE DEVELOPMENT

Analysis of the prediction curve generated in the landslide model shows that 41% of the testing landslides occurred in an area with 10% of the highest LSI values. And 62% of the testing landslides occurred in an area with 20% of the highest LSI values. In contrast, in the buffer zone model, 33% of the testing landslides occurred in the area with the 10% highest LSI values and 62% of the testing landslides occurred in the area with the 20% highest LSI values (Fig. 9). This comparison shows only a minimal advantage of the calculation model using landslides for calculations.

The predictive value of the model using buffer zones for calculations has been highlighted at the verification stage. The BSI map has been verified using test landslides, i.e. potential new landslides (62%) have been in the zones with the highest BSI values calculated using buffer zones. It gives a good indication of the location of potential future landslides.

The classes of passive factors with the highest BFR coefficients determine the slope parameters that have the greatest influence on the development of mass movements. Most of these classes, indicated by the use of buffer zones, were corroborated by the high LFR coefficients calculated using landslides. The model using buffer zones gives similar results to the methods using landslides.

Some parameters, especially the slope angle, have been more clearly emphasized by the buffer zones than by the landslides. The buffer zones highlighted the strong influence of slopes between 17–23° on the development of mass movements. Slopes with this inclination value dominated within the designated buffer zones. This value seems to be more probable in geological and relief conditions of the study area by comparison with the value of 35–52° indicated by the landslides model. The result of the landslide model differs significantly from previous studies carried out in other regions of the Carpathians, which indicated that slopes with an inclination of 3–22° are predisposed to the development of mass movements (Bober, 1990b; Zabuski et al., 1999; Kamiński, 2007; Wojciechowski, 2009; Wódka, 2022a; Kamieniarz, 2022) suggested that the number of landslides in the Carpathian Flysch decreases with increasing slope steepness above 25°. Therefore, the buffer zone model gives better results for the slope angle parameter.

CONCLUSIONS

In the present work, landslides and buffer zones have been used to calculate landslide susceptibility using the Frequency Ratio Model. Both calculation methods gave similar results, indicating that lithology, slope angle and distance from faults have the greatest influence on the formation of landslides in the Słonne Góry.

The use of buffer zones in the calculations did not improve the predictive values of the landslide susceptibility maps calculated using landslides as the standard. Instead, it gave very similar results. The value of the AUC index = 0.7971 indicates a sufficient (almost good) fit of the model, which is further confirmed by its verification using a group of testing landslides, up to 62% of which were located in the zones with the highest BSI. The predictive value of the landslide susceptibility map calculated using buffer zones is comparable to previous similar maps by Yesilnacar and Topal (2005) and Degdelenler et al. (2016). Maps, which were calculated using different methods of applying buffer zones to selected regions of Turkey, obtained the following ranges of AUC coefficients: 0.76–0.89 (Yesilnacar and Topal, 2005) and 0.783–0.792 (Degdelenler et al., 2016). During the construction of the landslide susceptibility map, the authors enriched the computational sets containing landslides with buffer values, without using the buffers themselves for calculations. Nevertheless, maps calculated in this way have a predictive value that is comparable to that of maps calculated using traditional methods.

The results of the present study are similar to those of Yilmaz (2007), who demonstrated the usefulness of buffer zones in landslide susceptibility mapping. Yilmaz (2007) used only buffer zones for his calculations. Unfortunately, he used the SCAI coefficient to validate the model, which emphasised the value of buffer zones designated above the main scarps. However, it is difficult to compare the predictive values of the two studies.

The studies cited demonstrate that the use of buffer zones has provided more effective conclusions regarding the real influence of certain classes of passive factors on the development of mass movements, while avoiding errors of interpretation. An example is the indication of a predisposed slope angle in the range of 17–23° instead of 35–52° in the process of landslide formation in the Słonne Góry.

In calculations of this type, the width of the designated buffer zones should depend on the specifics of the area under study, its relief, the length of the slopes, and the density of the stream network. The designated zones, 40 m wide, contained sufficient valuable data. This is consistent with the observations of Yilmaz (2007) and Dagdelenler et al. (2016) who concluded that the best data on landslide formation conditions was collected from 50 m-wide buffer zones, even though they had previously used wider buffers for their calculations. However, in the terrain of the Słonne Góry, a 50 m buffer produced too much erroneous data, so its width was reduced to 40 m.

In the western part of the Słonne Góry, the slopes made up of Godulian and radiolarian shales, Węglowiec veriegated marls, variegated shales and mudstones of the Menilite Beds,

are most prone to landslides. This is especially the case when the layers form folds at a distance of 100–250 m from their axes (especially from the axes of anticlines). The cataclinal slopes (dip slopes) with an aspect of N, NE, NW and a slope of 17–23° also favour the development of landslides. Mass movements commonly develop in zones 0-50 m from overthrusts and 0–200 m from faults.

Acknowledgements. This article presents the main sections of a Ph.D. Thesis, the public defence of which took place in June 2024 at the National Geological Institute – National Research Institute. The author would like to thank the editors and reviewers for constructive comments which helped to improve this manuscript.

REFERENCES

Akgun, A., 2012. A comparison of landslide susceptibility maps produced by logistic regression, multi-criteria decision, and likelihood ratio methods: a case study at İzmir, Turkey. Landslides, **9**: 93–106; https://doi.org/10.1007/s10346-011-0283-7

Bober, L., 1979. Zależność między rozwojem osuwisk strukturalnych, a budowa geologiczną Polskich Karpat fliszowych. (in Polish). Ph.D. Thesis, CAG Kraków, nr inw. 31597.

Bober, L., 1984. Landslide areas in the Polish Flysch Carpathians and their connection with the geological structure of the region (in Polish with English summary). Biuletyn Instytutu Geologicznego, **340**: 115–158.

Bober, L., 1985. Mapa osuwiskowości polskich Karpat fliszowych skala 1:200 000 (in Polish). CAG Warszawa, nr inw. 15997.

Bober, L., 1990a. Monografia osuwisk karpackich (in Polish). CAG Warszawa, nr inw. 303/91.

Bober, L., 1990b. Geologiczno-inżynierska klasyfikacja karpackich masywów fliszowych pod względem podatności na powstawanie osuwisk (in Polish). CAG Warszawa, nr inw. 375/91.

Carrara, A., Cardinali, M., Detti, R., Guzzettl, F., Pasqui, V., Reichenbach, P., 1991. GIS techniques and statistical models in evaluating landslide hazard. Earth Surface Processes and Landforms, **16**: 427–445.

Che, V.B., Kervyn, M., Suh, C.E., Fontijn, K., Ernst, G.G.J., del Marmol, M.-A., Trefois, P., Jacobs, P., 2012. Landslide susceptibility assessment in Limbe (SW Cameroon): a field calibrated seed cell and information value method. Catena, **92**: 83–98; https://doi.org/10.1016/j.catena.2011.11.014

Chen, W., Sun, Z., Zhao, X., Lei, X., Shirzadi, A., Shahabi, H., 2020. Performance evaluation and comparison of bivariate statistical-based artificial Intelligence algorithms for spatial prediction of landslides. International Journal of Geo-Information, **9:** 696–717; https://doi.org/10.3390/ijgi9120696

Chen, C.H., Ke, C.C., Wang, C.L., 2009. A back-propagation network for assessment of susceptibility to rock slope failure in the eastern portion of the Southern Cross-Island Highway in Taiwan. Environmental Geology, **57**: 723–733; https://doi.org/10.1007/s00254-008-1350-9

Cruden, D.M., Varnes, D.J., 1996. Landslides types and processes. TRB Spatial Reports, **274**: 36–75.

Degdelenler, G., Nefeslioglu, H.A., Gokceoglu, C., 2016. Modification of seed cell sampling strategy for landside susceptibility mapping: an application from Eastern part of the Gallipoli Peninsula (Canakkale, Turkey). Bulletin of Engineering Geology and the Environment, **75**: 575–590; https://doi.org/10.1007/s10064-015-0759-0

Dikau, R., Brunsden, D., Schrott, L., Ibsen, M.L., 1996. Landslide Recognition. Identification, Movement and Causes. John Wiley & Sons.

Długosz, M., 2011. Landslide susceptibility in the Polish Carpathians (in Polish with English summary). Prace Geograficzne, **230**.

Eeckhaut, M., Hervas, J., Jaedicke, C., Malet, J.-P., Montanarella, L., Nadim, F., 2012. Statistical modelling of Europe-wide landslide susceptibility using limited landslide inventory data. Landslides, **9**: 357–369; https://doi.org/10.1007/s10346-011-0299-z

Fayez, L., Thai Pham, B., Solanki, H.A., Pazhman, D., Dholakia, M.B., Khalid, M., Prakash, I., 2018. Application of frequency ratio model for the development of landslide susceptibility mapping at part of Uttarakhand State, India. International Journal of Applied Engineering Research, **13**: 6846–6854.

Gil, E., 1997. Meteorological and hydrological conditions of landslides, Polish flysch Carpathians. Studia Geomorphologica Carpatho-Balcanica, **31**: 143–158.

Gil, E., Długosz, M., 2006. Threshold values of rainfalls triggering selected deep-seated landslides in the Polish flysch Carpathians. Studia Geomorphologica Carpatho-Balcanica, **40**: 21–43.

Grabowski, D., Marciniec, P., Mrozek, T., Nescieruk, P., Rączkowski, W., Wójcik, A., Zimnal, Z., 2008. Instrukcja opracowania Mapy osuwisk i terenów zagrożonych ruchami masowymi w skali 1:10 000 (in Polish). Państwowy Instytut Geologiczny, Warszawa.

Grabowski, D., Laskowicz, I., Małka, A., Rubinkiewicz, J., 2022. Geoenvironmental conditioning of landsliding in river valleys of lowland regions and its significance in landslide susceptibility assessment: a case study in the Lower Vistula Valley, Northern Poland. Geomorphology, **419**, 108490; https://doi.org/10.1016/j.geomorph.2022.108490

Guzzetti, F., Carrara, A., Cardinali, M., Reichenbach, P., 1999. Landslide hazard evaluation: a review of current techniques and their application in a multi-scale study, Central Italy. Geomorphology, **31**: 181–216; https://doi.org/10.1016/S0169-555x(99)00078-1

Huang, J., Zhou, Q., Wang, F., 2015. Mapping the landslide susceptibility in Lantau Island, Hong Kong, by frequency ratio and logistic regression model. Annals of GIS, **21**: 191–208.

Hutchinson, J.N., 1968. Mass movement. In: Geomorphology. Encyclopedia of Earth Science. Springer, Berlin, Heidelberg; https://doi.org/10.1007/3-540-31060-6_238

Kamieniarz, S., 2022. Landslide susceptibility of Krakow city area (in Polish with English summary). Przegląd Geologiczny, **70**: 701–712; https://doi.org/10.7306/2022.24

Kamiński, M., 2007. Landslide susceptibility map: a case study from Jodłówka region (Dynowskie Foothills) (in Polish with English summary). Przegląd Geologiczny, **55**: 779–784.

Kamiński, M., 2012. Landslide susceptibility map in a region scale – example from of San Valley in the Dynów Foothills (in Polish with English summary). Biuletyn Państwowego Instytutu Geologicznego, **452**: 109–118.

Khan, H., Shafique, M., Khan, M.A., Bacha, M.A., Shah, S.U., Calligaris, C., 2019. Landslide susceptibility assessment using Frequency Ratio, a case study of northern Pakistan. The Egyptian Journal of Remote Sensing and Space Sciences, **22**: 11–24. https://doi.org/10.1016/j.ejrs.2018.03.004

Kleczkowski, A., 1955. Osuwiska i zjawiska pokrewne (in Polish). Wydaw. Geol., Warszawa.

Kos, J., 2019. Stability of landslide slopes based on inclinometer measurements and physical and mechanical properties of rocks and soils on the example of landslides in Ochojno and Stary Sącz (in Polish with English summary). Przegląd Geologiczny, **67**: 377–387; https://doi.org/10.7306/2019.32

Książkiewicz, M., 1972. Budowa geologiczna Polski. 4. Tektonika. 3. Karpaty (in Polish). Wydaw. Geol., Warszawa.

Lee, S., Prandhan, B., 2007. Landslide hazard mapping at Selangor, Malaysia using frequency ratio and logistic regression models. Landslides, **4**: 33–41; https://doi.org/10.1007/s10346-006-0047-y

Malata, T., Rączkowski, W., 1996. Objaśnienia do Szczegółowej mapy geologicznej Polski w skali 1:50 000, ark. Tyrawa Wołoska (1042) (in Polish). Państwowy Instytut Geologiczny, Warszawa.

Malata, T., Zimnal, Z., 2013. Objaśnienia do Szczegółowej mapy geologicznej Polski w skali 1:50 000, ark. Sanok (1041) (in Polish). Państwowy Instytut Geologiczny - PIB, Warszawa.

Malata, T., Zimnal, Z., 2014. Szczegółowa mapa geologiczna Polski w skali 1:50 000, ark. Sanok (1041) (in Polish). Państwowy Instytut Geologiczny - PIB, Warszawa.

Malata, T., Gucik, S., Rączkowski, W., Szymakowska, F., 2016. Szczegółowa mapa geologiczna Polski w skali 1:50 000, ark. Tyrawa Wołoska (1042) (in Polish). Państwowy Instytut Geologiczny - PIB, Warszawa.

Małka, A., 2015. Landslides susceptibility modeling using the index method and high-resolution airborne laser scanning data (LIDAR) in the area of Gdańsk (in Polish with English summary). Przegląd Geologiczny, **63**: 301–311.

Małka, A., 2021. Landslide susceptibility mapping of Gdynia using geographic information system-based statistical models. Natural Hazards, **107**: 639–374; https://doi.org/10.1007/s11069-021-04599-8

Margielewski, W., 2001. About the structural control of deep landslides. Implications for the Flysch Carpathians (southern Poland) (in Polish with English summary). Przegląd Geologiczny, **49**: 515–525.

Margielewski, W., 2009. Problems of structural landslides in the Polish Carpathians in the light of unified criteria of mass movement classifications – a critical review (in Polish with English summary). Przegląd Geologiczny, **57**: 905–917.

Mastella, L., 1975. Consequent-structural landslides from the Eastern Podhale (in Polish with English summary). Biuletyn Geologiczny UW, **18**: 259–270.

Mondal, S., Maiti, R., 2013. Integrating the Analytical Hierarchy Process (AHP) and the Frequency Ratio (FR) Model in landslide susceptibility mapping of Shiv-khola Watershed, Darjeeling Himalaya. International Journal of Disaster Risk Science, **4**: 200–212; https://doi.org/10.1007/s13753-013-0021-y

Mrozek, T., 2013. Landslide hazard and risk for a case-study of Szymbark region (Beskid Niski Mts) (in Polish with English summary). Prace Państwowego Instytutu Geologicznego, **199**: 5–40.

Mrozek, T., Poli, S., Sterlacchini, S., Zabuski, L., 2004. Landslide susceptibility assessment. A case study from the Beskid Niski Mts., Carpathians, Poland. Polish Geological Institute Special Papers, **15**: 13–18.

Mrozek, T., Laskowicz, I., Zabuski, L., Kulczykowski, M., Świdziński, W., 2016. Landslide susceptibility and risk assessment in a non-mountainous region – a case study of Koronowo, northern Poland. Geological Quarterly, **60**: 758–769; https://doi.org/10.7306/gq.1307

Nicu, I.C., 2018. Application of analytic hierarchy process, frequency ratio and statistical index to landslide susceptibility: an approach to endangered cultural heritage. Environmental Earth Sciences, **77**, 79. https://doi.org/10.1007/s12665-018-7261-5

Ou, P., Wu, W., Qin, Y., Zhou, X., Huangfu, W., Zhang, Y., Xie, L., Huang, X., Fu, X., Li, J., Jiang, J., Zhang, M., Liu, Y., Peng, S., Shao, C., Bai, Y., Zhang, X., Liu, X., Liu, W., 2021. Assessment of landslide hazard in Jiangxi using geo-information technology. Frontiers in Earth Science, **9**, 648342; https://doi.org/10.3389/feart.2021.648342

Pardeshi, S.D., Autade, S.E., Pardeshi, S.S., 2013. Landslide hazard assessment: recent trends and techniques. Springer Plus, **2**: 523–534.

Pradhan, B., Buchroithner, M. (eds.), 2012. Terrigenous Mass Movements. Detection, Modelling, Early Warning and Mitigation Using Geoinformation Technology. Springer, Berlin Heidelberg. https://doi.org/10.1007/978-3-642-25495-6

Przyłucka, M., Karkowska, K., 2022. Opady atmosferyczne a aktywność osuwiskowa w Karpatach (in Polish). Ogólnopolskiej Konferencji Osuwiskowej O!suwisko 18–21.10.2022, Kielnarowa

Rabby, Y.W., Li, Y., 2020. Landslide susceptibility mapping using integrated methods: a case study in the Chittagong Hilly Areas, Bangladesh. Geosciences, **10**, 483; https://doi.org/10.3390/geosciences10120483

Ramesh, V., Anbazahagan, S., 2015. Landslide susceptibility mapping along Kolli hills Ghat road section (India) using frequency ratio, relative effect and fuzzy logic models. Environmental Earth Sciences, **73**: 8009–8021; https://doi.org/10.1007/s12665-014-3954-6

Rączkowski, W., Mrozek, T., 2002. Activating of landsliding in the Polish Flysch Carpathians by end of the 20th century. Studia Geomorphologica Carpatho-Balcanica, **36**: 91–111.

Rycio, E., 2018. Geological conditions of the development of landslides in the Krynica-Zdrój region (in Polish with English summary). Przegląd Geologiczny, **66**: 294–302.

Sahana, M., Sajjad, H., 2017. Evaluating effectiveness of frequency ratio, fuzzy logic and logistic regression models in assessing landslide susceptibility: a case from Rudraprayag district, India. Journal of Mountain Science, **14**: 2150–2167; https://doi.org/10.1007/s11629-017-4404-1

Sikora, R., 2018. Structural control on the initiation and development of the Biała Wisełka Landslide Complex (Silesian Beskid, Outer Carpathians, Southern Poland). Geology, Geophysics & Environment **44**: 31–48; https://doi.org/10.7494/geol.2018.44.1.31

Silalahi, F.E.S., Pamela, Arifianti, Y., Hidayat, F., 2019. Landslide susceptibility assessment using frequency ratio model in Bogor, West Jawa, Indonesia. Geoscience Letters, **6**: 10–27; https://doi.org/10.1186/s40562-019-0140-4

Süzen, M.L., Doyuran, V., 2004. Data driven bivariate landslide susceptibility assessment using geographical information systems: a method and application to Asarsuyu catchment, Turkey. Engineering Geology, **71**: 303–321; https://doi.org/10.1016/S0013-7952(03)00143-1

Świątek, A., Indelak, K., Mikołajczyk, D., 2014. Wykorzystanie Indeksowej Metody Statystycznej w wyznaczaniu obszarów zagrożonych ruchami masowymi (in Polish). Prace Studenckiego Koła Naukowego Geografów Uniwersytetu Pedagogicznego w Krakowie, **3**: 111–126.

Świdziński, H., 1953. Karpaty fliszowe między Dunajcem a Sanem (in Polish). In: Regionalna Geologia Polski t. 1 Karpaty, z. 2 Tektonika (M. Książkiewicz). Polskie Towarzystwo Geologiczne, Kraków.

Van Westen, C.J., 1993. Application of geographic information systems to landslide hazard zonation. International Institute for Aerospace Survey and Earth Sciences, **15**.

Varnes, D.J., 1978. Slope movement types and processes. In: Landslides: Analysis and Control (ed. R.L. Schuster and R.J. Krizek): 11–35. Transportation Research Board, National Academy of Sciences, Washington.

Warmuz, B., Nescieruk, P., 2019. The dynamics of displacements of selected landslides in the Carpathians (in Polish with English summary). Przegląd Geologiczny, **67**: 326–331; https://doi.org/10.7306/2019.26

Wojciechowski, T., 2009. Geologiczna analiza osuwisk z wykorzystaniem satelitarnej interferometrii radarowej na przykładzie rejonu Nowego Sącza (in Polish). Ph.D. Thesis, Wydział Nauk o Ziemi Uniwersytetu Śląskiego.

Wojciechowski, T., 2019. Landslide susceptibility in Poland (in Polish with English summary). Przegląd Geologiczny, **67**: 320–325. https://doi.org/10.7306/2019.25

Wódka, M., 2019. The relationship between the selected landslide morphology and the geologic setting of the Carpathians and the Carpathian Foredeep based on the digital terrain model (in Pol-

ish with English summary). Przegląd Geologiczny, **67**: 115–122; https://doi.org/10.7306/2019.3

Wódka, M., 2022a. Conditions of landslide development during the last decade in the Rożnów Dam-Lake region (Southern Poland) based on Airborne Laser Scanning (ALS) data analysis. Geological Quarterly, **66**, 4; https://doi.org/10.7306/gq.1636

Wódka, M., 2022b. Lithological displacement index as an element of landslide susceptibility assessment (in Polish with English summary). Przegląd Geologiczny, **70**: 695–700; https://doi.org/10.7306/2022.23

Wójcik, A., 1997. Landslides in the Koszarawa drainage basin – structural and geomorphological control (Western Carpathians, Beskid Żywiecki Mts) (in Polish with English summary). Biuletyn Państwowego Instytutu Geologicznego, **376**: 5–42.

Wójcik, A., Zimnal, Z., 1996. Landslides along the San valley between Bachórzec and Reczpol (The Carpathian, The Carpathian Foreland) (in Polish with English summary). Biuletyn Państwowego Instytutu Geologicznego, **374**: 77–90.

WP/WLI, 1990. The International Geotechnical Societies` UNESCO Working Party for World Landslide Inventory. A suggested method for reporting a landslide. Bulletin of the Association of Engineering Geology, **41**: 5–12.

WP/WLI, 1993. The International Geotechnical Societies` UNESCO Working Party for World Landslide Inventory. Multilingual landslide glossary. The Canadian Geotechnical Society, BiTech Publishers Ltd, Rochmond BC, Canada: 1–7.

Yesilnacar, E., Topal, T., 2005. Landslide susceptibility mapping: a comparison of logistic regression and neural networks methods in a medium scale study, Hendek region (Turkey). Engineering Geology, **79**: 251–266; https://doi.org/10.1016/j.enggeo.2005.02.002

Yilmaz, C., 2007. GIS-Based landslide susceptibility mapping in Devrek (Zonguldak – Turkey). M.Sc. Thesis, Middle East Technical University in Ankara.

Youssef, A.M., 2015. Landslide susceptibility delineation in the Ar-Rayth area, Jizan, Kingdom of Saudi Arabia, using analytical hierarchy process, frequency ratio, and logistic regression models. Environmental Earth Sciences, **73**: 8499–8515; https://doi.org/10.1007/s12665-014-4008-9

Zabuski, L., Thiel, K., Bober, L., 1999. Landslides in Polish Carpathian Flysch. Geology-modelling-stability calculations (in Polish with English summary). Wydaw. IBW PAN, Gdańsk.

Zhang, Y.X., Lan, H.X., Li, L.P., Wu, Y., Chen, J., Tian, N., 2020. Optimizing the frequency ratio method for landslide susceptibility assessment: a case study of the Caiyuan Basin in the southeast mountainous area of China. Journal of Mountain Science, **17**: 340–357; https://doi.org/10.1007/s11629-019-5702-6

Ziętara, T., 1969. On the classification of landslides in the Western Beskids (in Polish with English summary). Studia Geomorphologica Carpatho-Balcanica, **3**: 111–130.

Ziętara, T., 1991. Influence of geological structure on landslide development in the Eastern part of the flysch Carpathians. Folia Geographica Series Geographica-Phisica, **22**: 71–86.

Ziętara, T., 2006. Issues in landslide forecasting and slope stabilisation in the Carpathians (in Polish with English summary). Problemy Zagospodarowania Ziem Górskich, **53**: 169–182.

APPENDIX 1
Summary of calculated coefficients for each class of passive factors

Layer Passive factor	Value class	LF *Landslides frequency*	BF *Buffer frequency*	CF *Class frequency*	LFR *Lanslides frequency ratio*	BFR *Buffer frequency ratio*
Lithology	Lower Krosno Beds – shale-sandstone flysch (17*)	0.0003	0.0005	0.001	0.232	0.305
	Lower Krosno Beds – sandstone – shale flysch (18*)	0.0003	0.002	0.056	0.006	0.034
	Lower Krosno Beds – Lesko sandstones (21*)	0.015	0.029	0.136	0.110	0.212
	Intermediate Beds (25*)	0	0.0002	0.0002	0	0.938
	Menilite Beds – mudstones (26*)	0.076	0.085	0.034	2.236	2.475
	Menilite Beds – cherts and Dynów marls (27*)	0.003	0.013	0.006	0.597	2.273
	Variegated shales (29*)	0.075	0.053	0.031	2.502	1.766
	Istebna sandstones (30*)	0.001	0.003	0.0003	3.356	11.025
	Węglowiec variegated marls (31*)	0.141	0.077	0.050	2.792	1.537
	Godula and radiolarian shales (32*)	0.129	0.076	0.029	4.497	2.638
	Upper Gaize Beds (33*)	0.319	0.401	0.206	1.549	1.949
	Lower Lgota Beds (34*)	0.026	0.04	0.036	0.738	1.111
	Verovice Beds (35*)	0.052	0.048	0.025	2.048	1.892
	Upper Krosno Beds – shale – sandstone flysch (37*)	0.096	0.095	0.249	0.385	0.383
	Upper Krosno Beds – sandstone – shale flysch (38*)	0.064	0.076	0.141	0.458	0.542

	Value class	LF	BF	CF	LFR	BFR
Bedding-slope relationship	Anaclinal (anti-dip)	0.052	0.052	0.077	0.674	0.673
	Plagioclinal (cross-dip)	0.632	0.624	0.641	0.985	0.974
	Cataclinal (dip)	0.185	0.186	0.155	1.189	1.198
	Transverse	0.131	0.137	0.126	1.039	1.087
Slope angle [°]	0-3	0.013	0.004	0.038	0.330	0.117
	3-6	0.089	0.039	0.141	0.627	0.275
	6-9	0.198	0.095	0.178	1.110	0.533
	9-12	0.183	0.150	0.183	1.003	0.822
	12-15	0.137	0.158	0.140	0.983	1.133
	15-17	0.108	0.163	0.097	1.119	1.688
	17-20	0.087	0.142	0.073	1.205	1.962
	20-23	0.067	0.106	0.056	1.206	1.909
	23-26	0.050	0.076	0.045	1.107	1.671
	26-30	0.034	0.043	0.031	1.114	1.416
	30-35	0.023	0.018	0.015	1.567	1.254
	35-52	0.009	0.002	0.003	2.839	0.746
Slope aspect	N	0.149	0.108	0.093	1.596	1.160
	NE	0.137	0.158	0.110	1.245	1.443
	E	0.066	0.098	0.092	0.712	1.070
	SE	0.071	0.113	0.104	0.690	1.088
	S	0.117	0.129	0.143	0.820	0.908
	SW	0.188	0.173	0.223	0.840	0.774
	W	0.151	0.130	0.152	0.995	0.857
	NW	0.121	0.089	0.083	1.460	1.072
Distance from overthrust [m]	0-50	0.089	0.056	0.034	2.627	1.661
	50-100	0.068	0.037	0.028	2.412	1.308
	100-150	0.051	0.026	0.026	1.965	1.016
	150-200	0.035	0.025	0.025	1.362	0.998
	200-250	0.025	0.030	0.025	0.972	1.178
	250-300	0.021	0.027	0.025	0.821	1.053
	300-350	0.020	0.023	0.025	0.798	0.921
	350-400	0.015	0.020	0.025	0.606	0.806
	400-500	0.016	0.029	0.051	0.311	0.569
	500-600	0.010	0.020	0.051	0.197	0.398
	600-1000	0.150	0.144	0.170	0.884	0.848
	>1000 m	0.487	0.537	0.401	1.215	1.341

	Value class	LF	BF	CF	LFR	BFR
Distance from faults [m]	0-50	0.080	0.033	0.029	2.729	1.118
	50-100	0.079	0.038	0.033	2.415	1.175
	100-150	0.075	0.038	0.036	2.078	1.049
	150-200	0.064	0.059	0.039	1.765	1.496
	200-250	0.054	0.052	0.040	1.353	1.296
	250-300	0.050	0.048	0.039	1.274	1.209
	300-350	0.045	0.044	0.039	1.154	1.122
	350-400	0.038	0.043	0.039	0.964	1.105
	400-500	0.049	0.073	0.077	0.633	0.950
	500-600	0.037	0.066	0.076	0.495	0.868
	600-1000	0.282	0.313	0.246	1.148	1.271
	>1000 m	0.139	0.192	0.305	0.458	0.631
Distance from anticline axis [m]	0-50	0.048	0.075	0.071	0.674	1.061
	50-100	0.068	0.083	0.068	1.001	1.218
	100-150	0.076	0.083	0.057	1.340	1.457
	150-200	0.069	0.075	0.044	1.594	1.728
	200-250	0.066	0.059	0.037	1.779	1.602
	250-300	0.051	0.036	0.031	1.636	1.129
	300-350	0.039	0.03	0.029	1.336	1.043
	350-400	0.026	0.026	0.026	1.017	1.009
	400-500	0.026	0.044	0.043	0.620	1.034
	500-600	0.012	0.021	0.031	0.379	0.670
	600-1000	0.013	0.015	0.057	0.227	0.273
	>1000 m	0.028	0.015	0.042	0.671	0.354
Distance from syncline axis [m]	0-50	0.065	0.065	0.067	0.967	0.972
	50-100	0.071	0.059	0.064	1.114	0.925
	100-150	0.061	0.054	0.055	1.117	0.993
	150-200	0.043	0.042	0.040	1.084	1.037
	200-250	0.028	0.024	0.033	0.865	0.736
	250-300	0.020	0.01	0.028	0.717	0.375
	300-350	0.021	0.015	0.025	0.824	0.581
	350-400	0.023	0.018	0.022	1.011	0.824
	400-500	0.041	0.035	0.036	1.130	0.966
	500-600	0.031	0.024	0.027	1.143	0.900
	600-1000	0.041	0.051	0.049	0.847	1.050
	>1000 m	0.029	0.036	0.086	0.336	0.423

*The numerical labels correspond to the numerical label on the geological layer presented in Figure 6

APPENDIX 2
Ranking of the highest LFR and BFR coefficients

Lp.	Class of passive factor	LFR	Class of passive factor	BFR
1	Godula and radiolarian shales	4.497	Godula and radiolarian shales	2.638
2	Istebna sandstones	3.356	Menilite Beds – mudstones	2.475
3	Slope angle 35-52º	2.839	Menilite Beds – cherts and Dynów marls	2.273
4	Węglowiec veriegated marls	2.792	Slope angle 17-20º	1.962
5	Fault dist. 0-50 m	2.729	Upper Gaize Beds	1.949
6	Overthrust dist. 0-50m	2.627	Slope angle 20-23º	1.909
7	Variegated shales	2.502	Verovice Beds	1.892
8	Fault dist. 50-100 m	2.415	Variegated shales	1.766
9	Overthrust dist. 50-100 m	2.412	Anticline dist. 150- 200 m	1.728
10	Menilite Beds – mudstones	2.236	Slope angle 15-17º	1.688
11	Fault dist. 100-150m	2.078	Slope angle 23-26º	1.671
12	Verovice Beds	2.048	Overthrust dist. 0-50 m	1.661
13	Overthrust dist. 100-150 m	1.965	Anticline dist. 200-250 m	1.602
14	Anticline dist. 200-250 m	1.779	Węglowiec veriegated marls	1.537
15	Fault dist.150-200 m	1.765	Fault dist. 150-200 m	1.496
16	Anticlines dist. 250-300 m	1.636	Anticline dist. 100-150 m	1.457
17	N	1.596	NE	1.443
18	Anticline dist. 150-200 m	1.594	Slope angle 26-30º	1.416
19	Slope angle 30-35º	1.567	Overthrust dist. 50-100 m	1.308
20	Upper Gaize Beds	1.549	Fault dist. 200-250 m	1.296
21	NW	1.46	Fault dist. 600-1000 m	1.271
22	Overthrust dist. 150-200 m	1.362	Slope angle 30-35º	1.254
23	Fault dist. 200-250 m	1.353	Anticline dist. 50-100 m	1.218
24	Anticline dist. 100-150 m	1.34	Fault dist. 250-300 m	1.209
25	Anticline dist. 300-350 m	1.336	Cataclinal	1.198
26	Fault dist. 250-300 m	1.274	Overthrust dist. 200-250 m	1.178
27	NE	1.2454	Fault dist. 50-100 m	1.175
28	Overthrust dist. above 3000 m	1.215	N	1.16
29	Slope angle 20-23º	1.206	Slope angle 12-15º	1.133
30	Slope angle 17-20º	1.205	Anticline dist. 250-300 m	1.129
31	Cataclinal	1.189	Fault dist. 300-350 m	1.122
32	Fault dist. 300-350 m	1.154	Fault dist. 0-50 m	1.118
33	Fault dist. 600-1000 m	1.148	Slope angle 0-3º	1.117
34	Syncline dist. 500-600 m	1.143	Lower Lgota Beds	1.111
35	Syncline dist. 400-500 m	1.130	Fault dist. 350-400 m	1.105
36	Slope angle 15-17º	1.119	SE	1.088
37	Syncline dist. 100-150m	1.117	Transverse	1.087
38	Syncline dist. 50-100 m	1.114	NW	1.072
39	Slope angle 26-30º	1.114	E	1.070
40	Slope angle 6-9º	1.110	Anticline dist. 0-50 m	1.061